# PERFORMANCE ANALYSIS OF MULTI-STRUCTURE CAPSULE ROBOTS DRIVEN BY PERMANENT MAGNETS

Yu Liu,* Liang Liang,* and Puhua Tang*

## Abstract

Capsule endoscopes (*i.e.*, capsule robots) are mainly used in the human gastrointestinal examination, especially small intestine. At present, the structure of capsule endoscopes in clinical application is the smooth capsule. Whether the spiral structure is conducive to improve the operational performance of capsule endoscopes without changing its operational stability needs to be further studied. In this paper, by the developed fluid field measuring system for magnetically driven capsule robots, the particle image velocimetry (PIV) technology is adopted to test the surrounding fluid velocity of capsule robots with different spiral pitches and groove depths. The computational fluid dynamics (CFD) method is further applied to calculate the fluid velocity and turbulent intensity around the capsule robot, the resistance and drag torque to the capsule robot in the moving direction, and the pressure on the pipe. The results show that the operational performance of the smooth capsule robot driven by permanent magnets is better than that of the spiral capsule robot. When the spiral pitch of the capsule robot is decreased and the spiral groove depth of the capsule robot is increased, the resistance and drag torque to the capsule robot, the surrounding fluid turbulent intensity and the maximum pressure on the pipe wall are all increased. The operational mode of precession will increase the energy consumption and operational instability of the capsule robot.

## Key Words

Smooth capsule robot, spiral capsule robot, spiral pitch, spiral groove depth, operational mode

## 1. Introduction

The endoscopes used to examine the health status of the human intestines are chronologically categorised into three main types. A manual endoscope [1] is suitable for intestinal examination in areas not far from the anus, which can easily cause harm to the human body and is relatively inexpensive. Human–machine cooperative endoscope [2], [3] is superior to manual endoscope, with relatively less damage. Its disadvantage is that it increases the size of the colonoscopy and makes it difficult to reach any position in the human intestines. Fully automatic capsule endoscope (*i.e.*, capsule robot) [4] has the advantage of minimal damage and can examine any position in the intestines. Its disadvantage is its high cost, and there is a risk of getting stuck in a certain position of the intestines when examining small sized intestines in children or lighter adults. The future development direction should be aimed at the capsule endoscope, reducing the size of capsule endoscope, optimising the structure of capsule endoscope, improving the control accuracy of outfield for capsule endoscope, realising the staying and posture adjustment at any position, expanding other functions of capsule endoscope, such as air blowing, drug release, surgery, *etc.*, and minimising the product cost.

According to the structure of the capsule robot, it can mainly be divided into the smooth cylindrical capsule robot [5], spiral capsule robot [6]–[9], claw type [10], needle type [11], leg type [12] or wheeled capsule robots [13], spherical capsule robot [14], deformable soft capsule robot [15], and separable capsule robot [16]. According to different structures, the functions of the capsule robot can be extended to positioning [17], sampling [18], releasing drugs [19], *etc.* The structure of the capsule robot usually corresponds to its function. At present, the capsule endoscope for clinical use is a smooth cylinder, which is used to cheque the intestine. The main functions of other structures are anchoring and dredging.

The driving modes of the capsule robot are divided into the wired driving mode and the wireless driving mode. The wired driving mode is mainly used for traditional endoscopes, but is not suitable for capsule endoscopes. The wireless driving mode mainly includes the internal battery drive and the external magnetic field drive [20]. The main problem of the battery is limited energy. Therefore, the external magnetic field is the most ideal driving mode. The magnetic field consists of the electromagnetic coils and permanent magnets [21]–[24]. The electromagnetic coils are

* College of Electromechanical Engineering, Changsha University, Changsha, China
  Corresponding author: Liang Liang

mainly multiple groups of Helmholtz coils that can generate the space magnetic field and drive the magnetic capsule robot. In this method, the magnetic field is uniform and the control is precise, but the equipment is complex and the control accuracy is high. The permanent magnets generate the magnetic force to drive the magnetic capsule robot. In this method, the equipment is simple, but the control accuracy is low.

The capsule robot system includes a pipe, mucus, and a capsule robot. The parameters related to the pipe mainly include: pipe shape, pipe surface morphology, and pipe diameter. The parameters related to mucus mainly include: fluid viscosity, fluid density, and fluid composition. The parameters related to the capsule robot mainly include: robot structural parameters, robot operational parameters, and external magnetic field parameters. The change of parameters related to the intestine is mainly to adjust the internal diameter of the intestine by changing the volume of mucus in the intestine. The parameters related to mucus are mainly changed by changing the concentration of medical silicone oil taken [25]. The parameters related to the capsule robot have become the focus and difficulties of current research, especially the numerous structural parameters of the robot, which have also become a challenge.

Zhou *et al.* [26] numerically calculated the moving velocity and drag torque of the outer spiral robot under different spiral parameters. Zhang *et al.* [27] measured the moving velocity and drag torque of capsule robots with different spiral parameters at the condition of mucus film of different thickness. Wang *et al.* [28] used the ANSYS-CFX tool to calculate and test the fluid speed at the pipe outlet when the outer spiral robot ran under different spiral parameters. Liang *et al.* [29] studied internal and external spiral robots, and numerically optimised the geometric parameters by using the orthogonal design method. Guo *et al.* [16] used the theoretical, numerical, and experimental methods to study the fluid pressure to the pipe wall when the robot rotated at the different speeds. Tang *et al.* [30] numerically calculated the effects of the moving speed, rotating speed, pipe diameter, and liquid viscosity on the operational performance indexes of the smooth robot, orthogonally analysed the weight and significance of these factors, and measured the fluid velocity around the robot. The research status related to the capsule robot system is shown in Table 1. The current research mainly calculates the influences of the spiral parameters of the robot on its running speed, drag torque and driving force, and measures the running speed of the robot and fluid speed. The theoretical research is mainly based on the contact mechanics and lubrication theory, and the numerical research is mainly based on the finite element method and finite volume method.

Considering that there is no theoretical and experimental comparative study on the structural parameters of the capsule robot driven by permanent magnet at present, this paper studies the performance indicators of the capsule robots with different structures when they runs in the pipe filled with fluid. The structures of
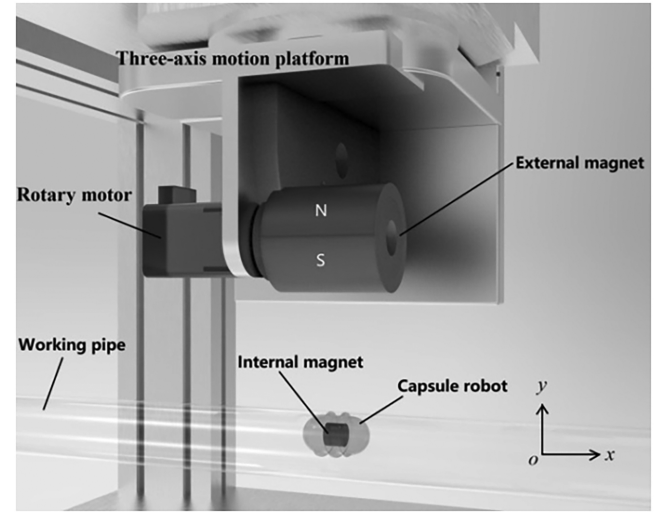


Figure 1. Schematic diagram of the magnetic drive system for capsule robot.

capsule robots have the smooth structure most commonly used in the intestinal capsule endoscope and the spiral structure that is expected to be used in medicine. The operational modes of capsule robots include translation and precession.

The influence of the two parameters (spiral pitch and groove depth) on the performance of the spiral robot is also studied. It provides a reference for the optimal design of the structure of the medical capsule endoscope driven by the permanent magnet.

## 2. Magnetic Drive System for Capsule Robot

In this paper, a magnetic drive system of capsule robot is designed by using the method of permanent magnet drive. In Fig. 1, the capsule robot with built-in cylindrical magnet is driven by the external annular permanent magnet. The external permanent magnet is driven by a three-axis motion platform, which makes a translational motion along the $x$, $y$, and $z$ axes. The rotary motor drives the external permanent magnet to rotate around its own central axis. Both the external and internal magnets are radially magnetised, and their north and south poles are opposite. When the external permanent magnet translates and rotates (precesses) along the $x$-axis, because of the magnetic force, the capsule robot will also make the same motion at the same speed in the pipe filled with mucus.

## 3. Fluid Measuring System for Capsule Robot

In order to compare the operational performance of capsule robots with different structures, a fluid measuring system for capsule robot is designed. The measuring system is to measure the flow field (velocity) of the fluid around the capsule robot when the capsule robot runs in a fluid-filled pipe, and verify the correctness of the theoretically calculated results.

Table 1
Research Status of the Capsule Robot System

| Capsule Robot System | Research Contents | | |
|---|---|---|---|
| Pipe | Pipe diameter [30] | | |
| Mucus | Fluid viscosity [30], fluid composition [29] | | |
| Capsule Robot | Main driving mode [20] | 1. Electromagnetic coils [21], [22] | |
| | | 2. Permanent magnets [23], [24] | |
| | Structure | Smooth cylinder [5], spiral [6]–[9] (spiral profile, pitch, groove depth, number of spiral), claw [10], needle [11], leg [12], wheel [13], sphere [14], deformable soft [15], separable [16] | |
| | Function | Positioning [17], sampling [18], releasing drugs [19] | |
| | Operational parameters | Translational speed, rotational speed | |
| | External field parameters | 1. Coil mode: Current frequency, phase, amplitude | |
| | | 2. Permanent magnet mode: Sizes of external and internal magnets, distance between the external magnet and capsule | |
| | Theoretical and numerical calculation | 1. Coil mode [25]–[27]: <br> ① Robot performance parameters: Robot surface pressure, robot propulsion speed, robot drag torque, and fluid velocity around the robot <br> ② Influencing factors: Rotational speed, spiral profile, spiral pitch, number of spiral, spiral groove depth, and minimum mucus film thickness | |
| | | 2. Permanent magnet mode [28], [29]: <br> ① Robot performance parameters: Robot axial thrust, circumferential drag torque, maximum pressure on pipe wall, fluid resistance, and fluid turbulent intensity around robot <br> ② Influencing factors: Solid phase size, concentration, liquid phase concentration, liquid phase distribution, internal and external spiral structure, spiral profile, spiral pitch, number of spiral, spiral groove depth, translational speed, rotational speed, viscosity of mucus, and pipe diameter | |
| | Experimental measurement | 1. Coil mode [25]–[27]: Robot's moving speed and fluid velocity | |
| | | 2. Permanent magnet mode (only smooth capsule) [28], [29]: Robot's moving speed, fluid velocity, and fluid vorticity around robot | |

Particle image velocimetry (PIV) technology is a transient, multi-point, non-contact measuring method of fluid velocity. The PIV technology is widely used in velocity field measurement of moving fluid. Considering the need of the PIV technology, the working pipe is a transparent round glass pipe, and the mucus is dimethyl silicone oil, which is equivalent to the intestinal fluid during capsule endoscope examination [25]. The density of the silicone oil is 975 kg/m³, and the dynamic viscosity is 0.1 Pa·s.

In Fig. 2, the fluid measuring system includes the robot module and the PIV module. The system can measure the fluid velocity at the *xoy* plane passing through the central axis of the robot. When the light directly irradiates the glass, because of the bigger density difference between air and glass, there will be refraction phenomenon of light, so the sheet-shaped light cannot be formed in the glass pipe. The brightness of the tracer particles will also be reduced, which will affect the imaging effect and lead to the big error of the PIV measurement. To avoid the above phenomenon, the glass pipe is put into a square glass tank, and a certain amount of tap water is poured into the tank to completely submerge the glass pipe. At this time, the light irradiates the bottom of the glass tank vertically. Because of the smaller density difference between water and glass, the light does not refract, and the light passes through the glass pipe to form the required sheet-shaped light. The outer diameters of the experimental capsules are 10–13 mm, their lengths are all 18 mm, and the surface material is bioplastics, which are similar in size and material to the capsule endoscopes in clinical practise [4].

## 4. Calculation Model of a Capsule Robot System

The theoretical calculation of the performance indicators of capsule robots with different spiral parameters is performed using the computational fluid dynamics (CFD) method.
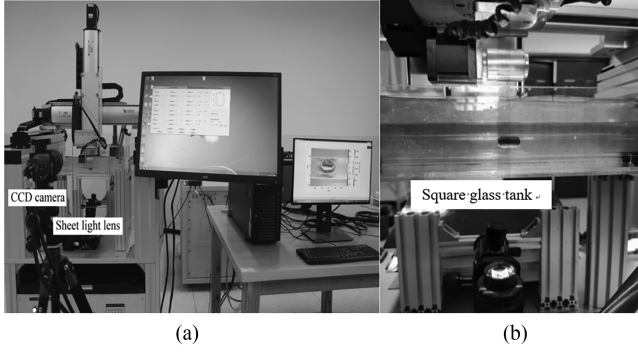
(a)       (b)

Figure 2. Fluid measuring system for capsule robot: (a) panoramic view of the system and (b) local view around the capsule robot.

## 4.1 Mathematical Model

When the capsule robot runs in a fluid-filled pipe, the fluid will exert forces on the capsule robot and the pipe wall. These forces can be obtained by calculating the fluid flow field (velocity and pressure) in the pipe. It is assumed that the fluid is not affected by temperature and is incompressible, and the fluid meets the basic laws of physics, namely, the mass conservation equation and momentum conservation equation [31]:

$$\frac{\partial \rho}{\partial t} + \nabla \cdot (\rho \boldsymbol{u}) = 0 \tag{1}$$

$$\begin{cases} \frac{\partial(\rho u_x)}{\partial t} + \nabla \cdot (\rho u_x \boldsymbol{u}) = -\frac{\partial p}{\partial x} + \frac{\partial \tau_{xx}}{\partial x} + \frac{\partial \tau_{yx}}{\partial y} + \frac{\partial \tau_{zx}}{\partial z} + F_x \\ \frac{\partial(\rho u_y)}{\partial t} + \nabla \cdot (\rho u_y \boldsymbol{u}) = -\frac{\partial p}{\partial y} + \frac{\partial \tau_{xy}}{\partial x} + \frac{\partial \tau_{yy}}{\partial y} + \frac{\partial \tau_{zy}}{\partial z} + F_y \\ \frac{\partial(\rho u_z)}{\partial t} + \nabla \cdot (\rho u_z \boldsymbol{u}) = -\frac{\partial p}{\partial z} + \frac{\partial \tau_{xz}}{\partial x} + \frac{\partial \tau_{yz}}{\partial y} + \frac{\partial \tau_{zz}}{\partial z} + F_z \end{cases} \tag{2}$$

where $\rho$ is the fluid density, $t$ is the time, $\nabla = \boldsymbol{i}\frac{\partial}{\partial x} + \boldsymbol{j}\frac{\partial}{\partial y} + \boldsymbol{k}\frac{\partial}{\partial z}$, $i$, $j$, and $k$ are the unit vectors of the $x$, $y$, and $z$ axes, $u_m$ ($m=x, y, z$) is component of fluid velocity vector $\boldsymbol{u}$ in the $x$, $y$, and $z$ directions, and $p$ is the fluid pressure, $\tau_{mn}$ ($m, n=x, y, z$) is component of viscous stress $\tau$ generated by viscosity of molecules, $F_m$ ($m=x, y, z$) is the volume force.

Equations (1) and (2) are the dynamic control equations of the viscous fluid, which are the mathematical models for fluid flow field calculation. It is difficult to obtain the analytical solution of the above partial differential equations. The CFD method can be used to solve the numerical solution that meets the practical requirements. The solution steps are as follows: The Pro/E software is used to establish the three-dimensional model of the capsule robot system, the Gambit software is used to divide the mesh and set the boundary conditions, and the ANSYS-Fluent software is used to set the solution parameters and solve numerically.

## 4.2 Structures and Parameters of Capsule Robots

We manufactured the smooth and spiral capsule robots. The spiral capsule robots are divided into two categories: one has different spiral pitches and the other has different spiral groove depths. For safety, the outer surface of the thread is designed as a semicircle. The parameters of capsule robots are shown in Table 2, and the pictures are shown in Fig. 3. As shown in Fig. 4, the diameter of the cylindrical magnets in the capsule robots is 6 mm, and the length is 5 mm. The internal magnet is bonded to other components of the capsule robot. The outside
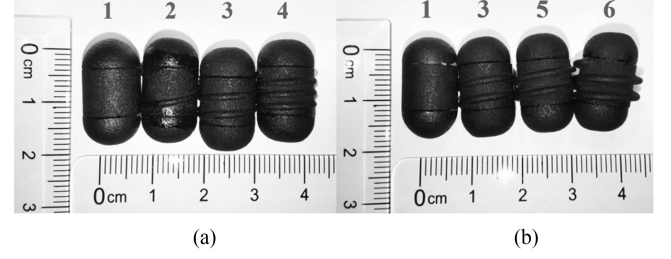


(a)       (b)

Figure 3. Capsule robots with different structures and parameters: (a) different spiral pitches and (b) different spiral groove depths.
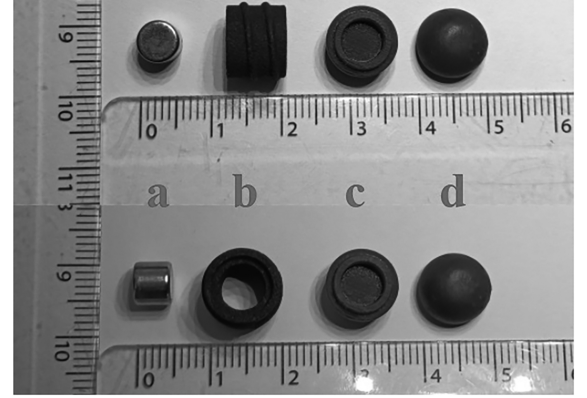


Figure 4. Exploded view of the capsule robot parts: (a) internal magnet; (b) middle spiral end; (c) front end cover; and (d) rear end cover.

diameter of the external permanent magnet is 28 mm, the inside diameter is 12 mm, and the length is 30 mm. The internal and external magnets are all made of NdFeB. The distance of the axes of the capsule robot and the external magnet is constant and fixed at 51 mm. According to our previous work [32], it can be measured that the magnetic force between them is about 0.2 N.

## 4.3 Computational Domain and Grid of the Capsule System

The capsule robot system studied is divided into the pipe, mucus, and capsule robot. The pipe is a straight pipe with a diameter of 18 mm and a length of 300 mm. The computational domain of fluid in the pipe for the capsule robot (No. 3) system is divided into internal domain and external domain, as shown in Fig. 5. The internal domain is a thin fluid with a thickness of 1 mm wrapped around the capsule, and the external domain is the remaining fluid. Unstructured tetrahedral grids are used in the two domains, and the grid of the internal domain is refined.

When the grid quality meets the calculation requirements (*i.e.,* the quality value of the worst grid element in all domains is less than 0.8), taking the circumferential drag torque of the capsule robot as the evaluation index, the grid number is increased and the time step is decreased until the index tends to be steady. Fig. 6 shows the computational results of grid independence verification for the capsule robot. When the total number of grids reaches 270,000, the target value tends to be stable. Finally, the total number of grids is

Table 2
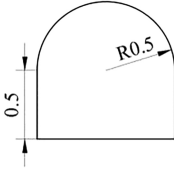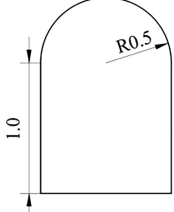Parameter Values of Capsule Robots with Different Structures

| No. | Structure | Thread Profile | Spiral Groove Depth $e$ (mm) | Effective Length of Thread (mm) | Spiral Pitch $h$ (mm) | Number of Spiral | Length (mm) | Diameter (mm) |
|---|---|---|---|---|---|---|---|---|
| 1 | Smooth | 0 | 0 | / | $\infty$ | / | 18 | 10 |
| 2 | Spiral | R0.5 | 0.5 | 6 | 6 | 1 | | |
| 3 | | | | | 3 | | | |
| 4 | | | | | 2 | | | |
| 5 | | R0.5 / 0.5 | 1.0 | | 3 | | | |
| 6 | | R0.5 / 1.0 | 1.5 | | | | | |



Figure 5. Computational domains of the fluid in the pipe for the capsule robot (No. 3): (a) overall view of the robot system and (b) enlarged view of the robot.

273,347 and the time step is 0.0005 s. The divided grid is shown in Fig. 7.

### 4.4 Turbulent Model and Boundary Conditions

The standard $k$-$\varepsilon$ turbulent model is chosen, and the standard wall function is used. The inlet and outlet of the pipe are all set as walls, and the fluid flow is not considered. According to the actual condition, the robotic translational speed ($v$) is set as 0.04 m/s, and the robotic rotational speed ($n$) is set as 120 r/min. The gravity of the fluid is considered, and the direction is negative along the $y$-axis. The gravity of the robot is not considered because the robot is in equilibrium in the pipe. The standard SIMPLE algorithm is used to solve the pressure and velocity coupling equations of the fluid flow field. The difference schemes of pressure, momentum, turbulent kinetic energy, and dissipation rate are all second-order upwind schemes.

Because of the rotation and translation of the robot, the sliding mesh method and dynamic mesh technique are used to simulate the rotational and translational motion, respectively, and the capsule robot is assumed to precess along the $x$-axis. The whole numerical calculation is transient calculation. The initial condition is set to zero for all regions. The convergence accuracy of the solution is: continuity, velocity in $x$, $y$, and $z$ axial directions, $k$ and $\varepsilon$ are all 0.001.

### 5. Results and Analysis

Firstly, the experimental measurement results and theoretical calculation results are compared and analysed, and the influence of the spiral parameters of capsule robots on the
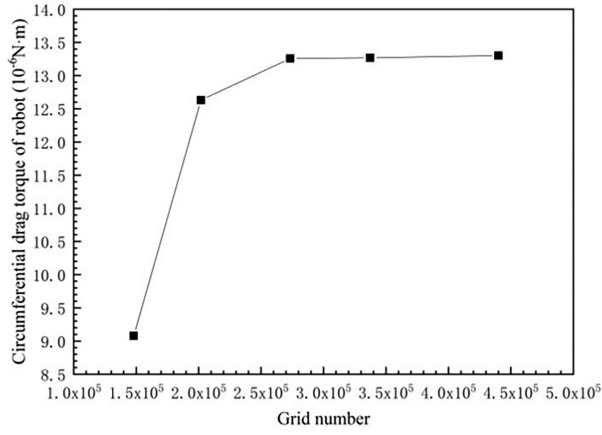
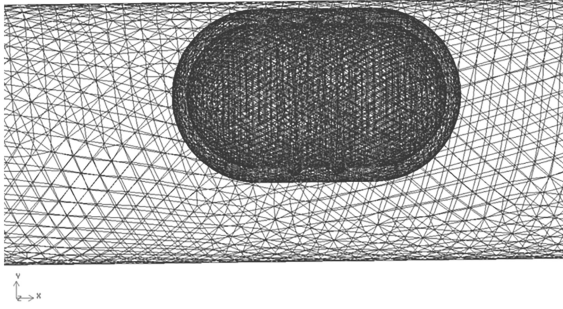Figure 6. Computational domain grid of the robot system.



Figure 7. Grid independence analysis of the robot system.



Figure 8. Reference coordinate origin for quantitative analysis.

performance indicators of capsule robots is then further discussed.

## 5.1 Experimental Verification of the Numerical Calculation

The PIV technology is used to measure the fluid flow field (velocity and vorticity [33]) when the capsule robot runs in the pipe filled with silicone oil. In the experiment, the external annular permanent magnet makes a precessing motion along the $x$-axis, the translational speed is 0.04 m/s, the rotational speed is 120 r/min, and drives the capsule robot to make the same motion at the same speeds. The reason for choosing the No. 3 capsule robot with a smaller spiral groove depth (0.5 mm) and moderate spiral pitch (3 mm) as the experimental object is that when the spiral groove depth of the capsule robot is larger, the operational stability of the capsule robot in the pipe filled with fluid is decreased, and the spiral pitch of the capsule robot has a smaller impact on the operational performance of the capsule robot. To quantitatively compare the calculated and experimental values, as shown in Fig. 8, a set of rectangular coordinate system is established, and the coordinate origin is set at the bottom centre of the capsule. This coordinate system moves with the capsule robot, the translational speed of the coordinate system is the same as that of the robot, and the rotational speed is zero. Fig. 9 shows the pictures of the capsule robot in the pipe at different times, and the translational speed of the capsule robot is also 0.04 m/s.

Fig. 10 shows the $x$-component of the fluid velocity and vorticity around the $z$-axis on the $y$-axis below the coordinate origin. The velocity of the fluid below the capsule robot along the $x$-axis (i.e. the moving direction of the capsule robot) is
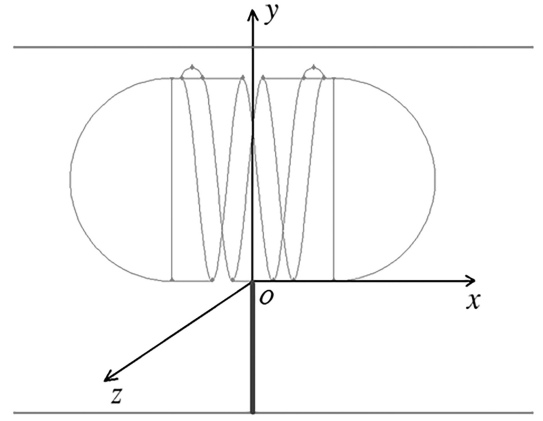
negative, that is, the direction of fluid velocity is opposite to the moving direction of the robot. The vorticity of the fluid around $z$-axis below the capsule robot is changed from negative to positive, that is, the rotational direction of the fluid around the $z$-axis is changed from clockwise to anticlockwise. The rotational intensity at the fluid zones adjacent to the capsule robot and the pipe is greater, while the rotational intensity at the fluid zone between the capsule robot and the pipe is smaller. Comparing the numerical and experimental results, the change trend and values of the two are similar, which proves that the CFD method used in this paper is reasonable and effective.

## 5.2 Operational Performance Analysis of Multi-Structure Capsule Robots

When capsule robots with different structures and parameters translate or precess in a pipe filled with mucus, their operational performance will affect the reasonable selection of structures and parameters. This paper focuses on the spiral pitch ($h$) and spiral groove depth ($e$) of the capsule robot. The operational performance indexes of the capsule robot are defined as follows: the resistance of the robot in the moving direction ($F_r$, reflecting the difficulty of the robot passing through the pipe); the circumferential drag torque of the robot in the moving direction ($T_r$, reflecting the energy consumption and twisting force of the robot); the fluid turbulent intensity [29] around the robot ($I$, reflecting the operational stability of the robot); and the maximum pressure on the pipe wall ($P_{max}$, reflecting the damage degree of the pipe caused by the robot).

### 5.2.1 Spiral Pitch

As shown in Fig. 3(a) and Table 2, the spiral pitches of the four capsule robots (No. 1, 2, 3, and 4) are $\infty$ (smooth), 6 mm, 3 mm, and 2 mm, respectively. Figures 11–14 show the change of the operational performance indexes of the robot with the reciprocal ($1/h$) of the spiral pitch when the capsule robot precesses or translates. These figures show that whether the capsule robot driven by permanent magnets precesses or translates, with the decrease of the spiral pitch of the robot, the resistance and drag torque of the robot in the moving direction and the maximum pressure on the pipe wall are all increased, and the fluid turbulent intensity around the
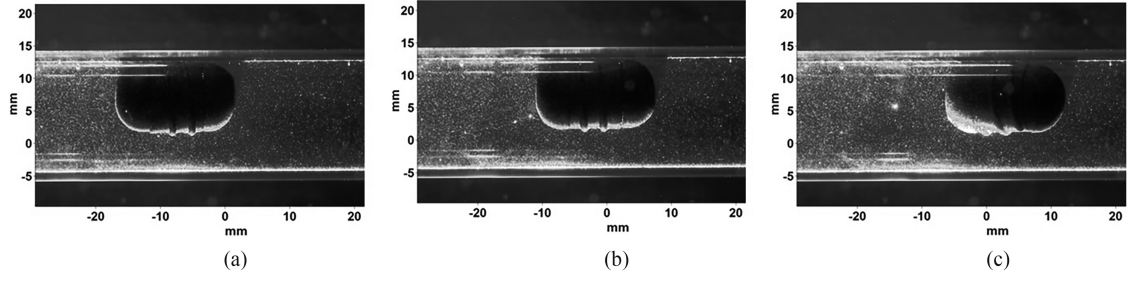
Figure 9. Pictures of the capsule robot at different times: (a) $t = 0$ s; (b) $t = 0.125$ s; and (c) $t = 0.25$ s.
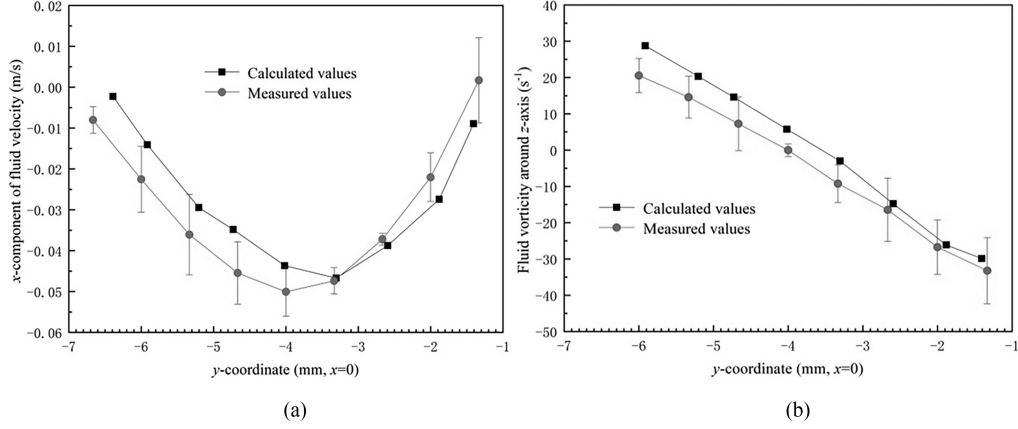


Figure 10. Fluid field around capsule robot No. 3 ($v = 0.04$ m/s, $n = 120$ r/min): (a) $x$-component of velocity and (b) vorticity around $z$-axis.
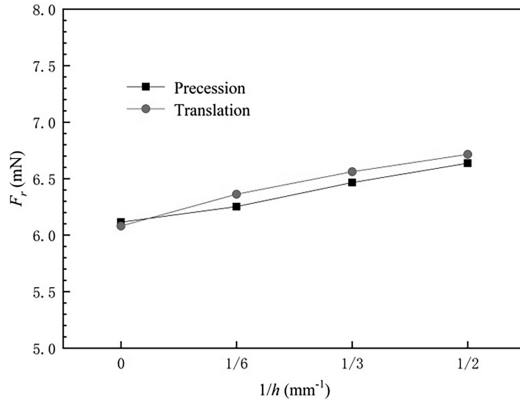


Figure 11. Relationship between $F_r$ and $1/h$.
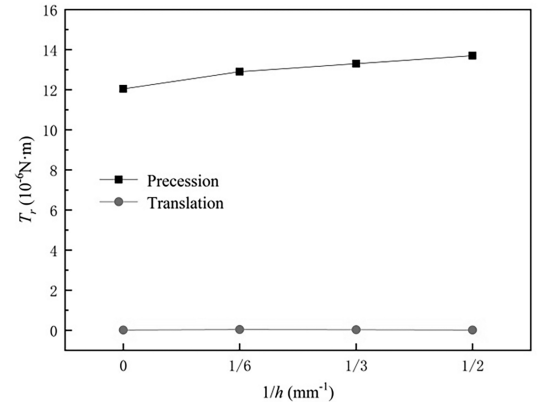


Figure 12. Relationship between $T_r$ and $1/h$.

capsule robot is firstly increased and then remains unchanged. So the spiral capsule robot with smaller spiral pitches is more hindered by the fluid when translating or rotating in the pipe, and the damage to the pipe wall is greater. The operation of spiral capsule robot is more unstable than that of smooth capsule robot, and the operational stability of the spiral capsule robots with different spiral pitches are almost the same.

For the capsule robots with different spiral pitches, the forwards resistance of the robots and the maximum pressure on the pipe wall for the precessing mode are the same as those for the translating mode. For the capsule robots with different spiral pitches, the drag torque in the robotic moving direction and the fluid turbulent intensity around the

robots are bigger for the precessing mode than those for the translating mode.

### 5.2.2 Spiral Groove Depth

As shown in Fig. 3(b) and Table 2, the spiral groove depths of the four capsule robots (No. 1, 3, 5, and 6) are 0 (smooth), 0.5 mm, 1 mm, and 1.5 mm, respectively. Figures 15–18 show the change of the operational performance indexes of the robot with the spiral groove depths when the capsule robot precesses or translates. These figures show that with the increase of the spiral groove depth of the robot, the resistance and drag torque of the robot in the moving direction, the fluid turbulent intensity around the robot, and
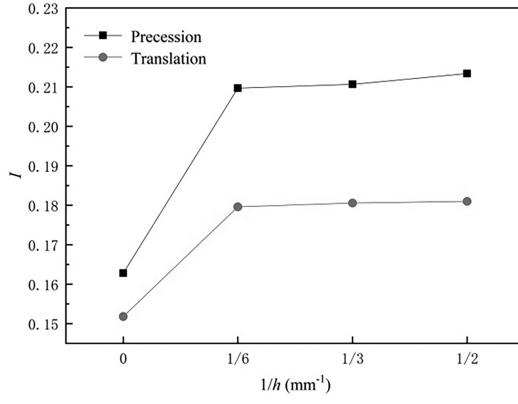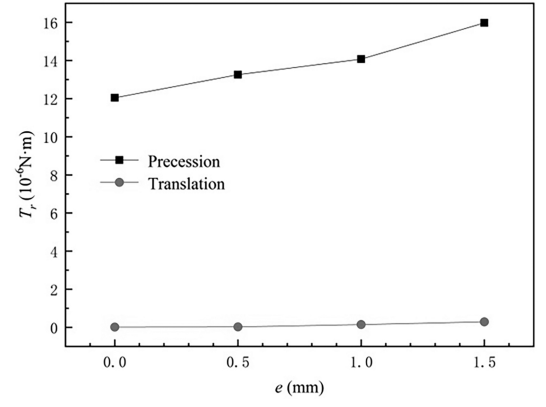
Figure 13. Relationship between $I$ and $1/h$.



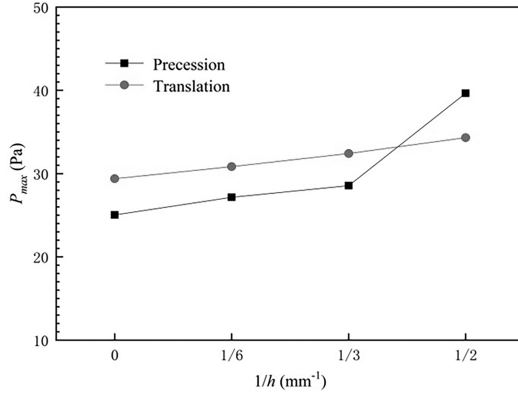Figure 14. Relationship between $P_{\max}$ and $1/h$.
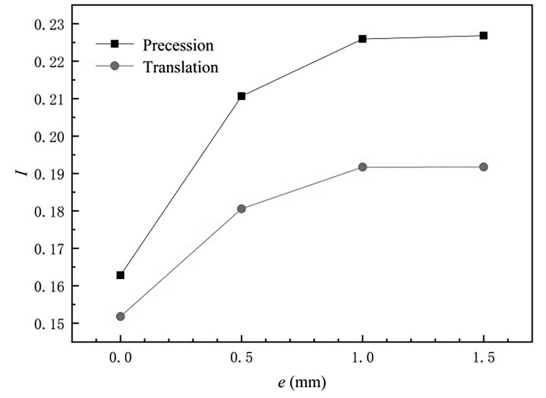


Figure 15. Relationship between $F_r$ and $e$.
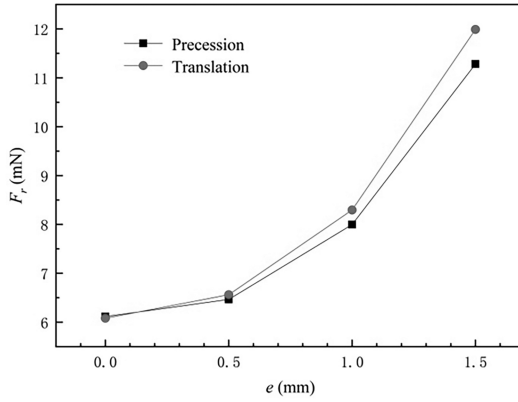


Figure 16. Relationship between $T_r$ and $e$.
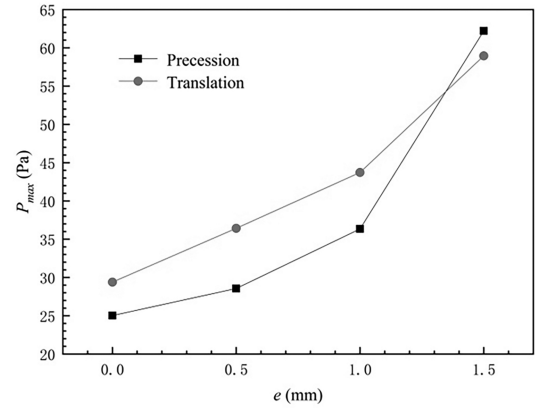


Figure 17. Relationship between $I$ and $e$.



Figure 18. Relationship between $P_{\max}$ and $e$.

the maximum pressure on the pipe wall are increased whether it is precession or translation for the capsule robot driven by the permanent magnets. It is indicated that the spiral capsule robot with larger groove depths is more hindered by the fluid when translating and rotating in the pipe, the operation is more unstable, and the damage to the pipe wall is greater.

For the capsule robots with different spiral groove depths, the resistance in the moving direction and the maximum pressure on the pipe wall for the precessing mode are the same as those for the translating mode, which indicates that the operational mode (precession or translation) of the capsule

robot driven by permanent magnets has little effect on the resistance of the robot and the maximum pressure on the pipe wall, which is similar to that for the capsule robots different spiral pitches. For the capsule robots with different spiral groove depths, the drag torque in the moving direction and the fluid turbulent intensity around the robots for the precessing mode are bigger than those for the translating mode, which shows that the capsule robot runs more unstable and has greater twisting force and energy consumption for the precessing mode.

When a spiral capsule robot with a smaller pitch and a larger groove depth precesses in the intestine, the torque

of the robot generated by the rotating external permanent magnet is greater, making it easy to pass through some positions with high frictional forces. Smooth capsule structure is preferred for intestinal examination compared to spiral capsule structure, because it can reduce the fluid resistance, running instability and damage to the intestine during operation.

## 6. Conclusion

In this paper, we developed a measuring system of fluid flow field for the capsule robot driven by permanent magnets, combined with the CFD method, and studied the operational performance of capsule robots with different structures and spiral parameters in order to optimize the structure of the clinical capsule endoscope. For the capsule robot driven by permanent magnets, because the driving force of the capsule robot comes from the magnetic force of the external magnet, compared with the spiral capsule robot, the smooth capsule robot suffers the smaller resistance, drag torque, fluid turbulent intensity around the robot and the maximum pressure on the pipe wall. Considering the longer length and more curved parts of the human intestine, a capsule endoscope is more suitable for examining the entire intestine than a traditional endoscope. When there are more impurities or insufficient liquid in the intestine, the frictional force between the capsule and the intestine is high, and there is a risk of the capsule not being able to pass through it. At this time, a spiral capsule with a smaller pitch and a larger groove depth can be used. When it precesses, the torque of the spiral capsule robot is greater, making it easy to pass through the entire intestine. Therefore, when fully excluding intestinal impurities or filling the intestine with sufficient liquid, the smooth structure should be preferentially selected for the capsule endoscope driven by permanent magnets. Compared with the translating mode, the precessing mode will increase the forwards drag torque of the capsule robot and the surrounding fluid turbulent intensity. This work will be very beneficial for the future application of the new structural capsule endoscopes with different requirements.

## Acknowledgement

## References

[1] F.Y. Araghizadeh, A.E. Timmcke, F.G. Opelka, T.C. Hicks, and D.E. Beck, Colonoscopic perforations, *Diseases of the Colon and Rectum*, *44*, 2001, 713–716.

[2] W.B. Cheng, Y.Y. Di, E.M. Zhang, M.A. Moser, S. Kanagaratnam, L.Y. Korman, N. Sarvazyan, and W.J. Zhang, Modelling and in vitro experimental validation for kinetics of the colonoscope in colonoscopy, *Annals of Biomedical Engineering*, *41*, 2013, 1084–1093.

[3] W.B. Cheng, M.A.J. Moser, and S. Kanagaratnam, Predication for relative motion of the colonoscope in colonoscopy, *Journal of Mechanics in Medicine and Biology*, *13*(3), 2013, 1350023.

[4] Z. Liao, Z.S. Li, and Z.D. Jin, *Mapping of gastrointestinal remote capsule endoscopy*, (Beijing: Tsinghua University Press, 2015).

[5] G. Iddan, G. Meron, A. Glukhovsky, and P. Swain, Wireless capsule endoscopy, *Nature*, *405*, 2000, 417.

[6] W.B. Cheng, M. Moser, S. Kanagaratnam, and W.J. Zhang, Development of autonomous microrobotics in endoscopy, *Journal of Medical Engineering and Technology*, *35*(8), 2011, 391–401.

[7] L. Zheng, S. Guo, and Z. Wang, Performance evaluation of an outer spiral microrobot in pipes in different environments, *Proc. 2020 IEEE International Conf. on Mechatronics and Automation (ICMA)*, Beijing, China, 2020, 643–647.

[8] Y. Zhang, H. Yang, D. Yang, X. Liu, and Z. Liu, Polynomial profile optimisation method of a magnetic petal-shaped capsule robot, *Mechatronics*, *65*, 2020, 102309.

[9] L. Liang, R. Hu, B. Chen, Y. Tang, and Y. Xu, Scaling effects in spiral capsule robots, *Proceedings of the Institution of Mechanical Engineers Part H: Journal of Engineering in Medicine*, *231*(4), 2017, 307–314.

[10] M.N. Huda, P. Liu, C. Saha, and H. Yu, Modelling and motion analysis of a pill-sized hybrid capsule robot, *Journal of Intelligent and Robotic Systems*, *100*, 2020, 753–764.

[11] A. Mousa, L. Feng, Y. Dai, and O. Tovmachenko, Self-driving 3-legged crawling prototype capsule robot with orientation controlled by external magnetic field, *Proc. 2018 WRC Symp. on Advanced Robotics and Automation (WRC SARA)*, Beijing, China, 2018, 243–248.

[12] D. Han, G. Yan, Z. Wang, P. Jiang, D. Liu, K. Zhao, and J. Ma, The modelling, analysis, and experimental validation of a novel micro-robot for diagnosis of intestinal diseases, *Micromachines*, *11*, 2020, 896.

[13] M.C. Hoang, V.H. Le, J. Kim, E. Choi, and CS. *Kim*, Untethered robotic motion and rotating blade mechanism for actively locomotive biopsy capsule endoscope, *IEEE Access*, *7*, 2019, 93364–93374.

[14] H. Yang, Y. Zhang, and X. Liu, Dynamic characteristics analysis of a magnetically driven dual hemisphere capsule robot by eccentric gravity centre, *Proc. 2020 5th International Conf. on Automation, Control and Robotics Engineering (CACRE)*, Dalian, China, 2020, 101–109.

[15] S. Yim, K. Goyal, and M. Sitti, Magnetically actuated soft capsule with the multimodal drug release function, *IEEE/ASME Transactions on Mechatronics*, *18*(4), 2013, 1413–1418.

[16] J. Guo, Z. Bao, Q. Fu, and S. Guo, Design and implementation of a novel wireless modular capsule robotic system in pipe, *Medical and Biological Engineering and Computing*, *58*, 2020, 2305–2324.

[17] S.Y. Yen, H.E. Huang, and H.C. Chen, A novel method for locating a magnetic-assisted capsule endoscope system, *IEEE Transactions on Magnetics*, *56*(10), 2020, 1–6.

[18] D. Son, H. Gilbert, and M. Sitti, Magnetically actuated soft capsule endoscope for fine-needle biopsy, *Soft Robotics*, *7*(1), 2020, 10–21.

[19] J. Lee, H. Lee, S. Kwon, and S. Park, Active delivery of multi-layer drug-loaded microneedle patches using magnetically driven capsule, *Medical Engineering and Physics*, *85*, 2020, 87–96.

[20] Z. Li, C. Li, L. Dong, and J. Zhao, A review of microrobot's system: Towards system integration for autonomous actuation in vivo, *Micromachines*, *12*(10), 2021, 1249.

[21] L. Manamanchaiyaporn, T. Xu, and X. Wu, Roles of magnetic strength in magneto-elastomer towards swimming mechanism and performance of miniature robots, *International Journal of Robotics and Automation*, *35*(2), 2020, 162–170.

[22] M. Chi, R. Liu, C. Chang, and W. Yuanli, Bivariable magnetic moment control of a capsule endoscope, *International Journal of Robotics and Automation*, *37*(6), 2022, 512–519.

[23] J. Li, E.S. Barjuei, and G. Ciuti, Magnetically-driven medical robots: An analytical magnetic model for endoscopic capsules design, *Journal of Magnetism and Magnetic Materials*, *452*, 2018, 278–287.

[24] G. Pittiglio, L. Barducci, J.W. Martin, J.C. Norton, C.A. Avizzano, K.L. Obstein, and P. Valdastri, Magnetic levitation for soft-tethered capsule colonoscopy actuated with a single permanent magnet: A dynamic control approach, *IEEE Robotics and Automation Letters*, *4*(2), 2019, 1224–1231.

[25] X. Liu, Y. Han, and G. Wu, Dimethicone power applied under endoscopy in examination of upper gastrointestinal tract, *China Journal of Endoscopy*, *22*(6), 2016, 44–46.

[26] H. Zhou, G. Alici, T.D. Than, and W. Li, Modeling and experimental characterization of propulsion of a spiral-type microrobot for medical use in gastrointestinal tract, *IEEE Transactions on Biomedical Engineering*, *60*(6), 2012, 1751–1759.

[27] Y. Zhang, H. Yang, D. Yang, X. Liu, and Z. Liu, Polynomial profile optimization method of a magnetic petal-shaped capsule robot, *Mechatronics*, *65*, 2020, 102309.

[28] Z. Wang, S. Guo, Q. Fu, and J. *Guo*, Characteristic evaluation of a magnetic-actuated microrobot in pipe with screw jet motion, *Microsystem Technologies, 25*, 2019, 719–727.

[29] L. Liang, B. Chen, Y. Tang, Y. Xu, and Y. Liu, Operational performance analysis of spiral capsule robot in multiphase fluid, *Robotica*, *37*(2), 2019, 213–232.

[30] P. Tang, L. Liang, Z. Guo, Y. Liu, and G. Hu, Orthogonal optimal design of multiple parameters of a magnetically controlled capsule robot, *Micromachines*, *12*, 2021, 802.

[31] F. Wang, *Computational fluid dynamics analysis - CFD software theory and application*, (Beijing: Tsinghua University Press, 2004).

[32] Z. Guo, L. Liang, and D. Lin, Modeling and measurement of magnetic driving force in the capsule robot, *Chinese Journal of Scientific Instrument*, *43*(1), 2022, 253–261.

[33] J. Li, H. Zhang, and H. Zhang, Numerical simulation on vortical structures of electrolyte flow field in large aluminium reduction cells, *Chinese Journal of Nonferrous Metals*, *22*(7), 2012, 2082–2089.

## Biographies

*Yu Liu* was born in 1978. He received the Ph.D. degree in materials engineering from Central South University, Changsha, China, in 2016. He is currently an Associate Professor with the College of Electromechanical Engineering, Changsha University, Changsha, China. His research interests include robotics technology, mould flow analysis and powder injection moulding.



*Liang Liang* was born in 1977. He received the Ph.D. degree in automation from Central South University, Changsha, China, in 2012. He is currently a Professor with the College of Electromechanical Engineering, Changsha University, Changsha, China. His research interests include robotics technology, fluid flow analysis, and fluid mechanical wear.



*Puhua Tang* was born in 1973. He is currently an Associate Professor with the College of Electromechanical Engineering, Changsha University, Changsha, China. His research interests include fluid flow analysis and hydraulic technology.